Earth and Planetary Science Letters 302 (2011) 287–298

Contents lists available at ScienceDirect

Earth and Planetary Science Letters

journal homepage: www.elsevier.com/locate/epsl

A model for seismicity rates observed during the 1982–1984 unrest at Campi Flegrei caldera (Italy)

M.E. Belardinelli [a,*], A. Bizzarri [b], G. Berrino [c], G.P. Ricciardi [c]

[a] Università degli Studi di Bologna, Dipartimento di Fisica, Bologna, Italy
[b] Istituto Nazionale di Geofisica e Vulcanologia, Sezione di Bologna, Bologna, Italy
[c] Istituto Nazionale di Geofisica e Vulcanologia, Sezione di Napoli Osservatorio Vesuviano, Napoli, Italy

ARTICLE INFO

Article history:
Received 17 June 2010
Received in revised form 3 December 2010
Accepted 7 December 2010
Available online 8 January 2011

Editor: Y. Ricard

Keywords:
stress triggering
bradyseism
rate- and state-dependent friction
variable stressing rates
Coulomb stress

ABSTRACT

We consider the space–time distribution of seismicity during the 1982–1984 unrest at Campi Flegrei caldera (Italy) where a correlation between seismicity and rate of ground uplift was suggested. In order to investigate this effect, we present a model based on stress transfer from the deformation source responsible for the unrest to potential faults. We compute static stress changes caused by an inflating source in a layered half-space. Stress changes are evaluated on optimally oriented planes for shear failure, assuming a regional stress with horizontal extensional axis trending NNE-SSW. The inflating source is modeled as inferred by previous studies from inversion of geodetic data with the same crustal model here assumed. The magnitude of the regional stress is constrained by imposing an initial condition of "close to failure" to potential faults. The resulting spatial distribution of stress changes is in agreement with observations. We assume that the temporal evolution of ground displacement, observed by a tide-gauge at Pozzuoli, was due mainly to time dependent processes occurring at the inflating source. We approximate this time dependence in piecewise-linear way and we attribute it to each component of average stress-change in the region interested by the observed seismicity. Then we evaluate the effect of a time dependent stressing rate on seismicity, by following the approach indicated by Dieterich (1994) on the basis of the rate- and state-dependent rheology of faults. The seismicity rate history resulting from our model is in general agreement with data during the period 1982–1984 for reasonable values of unconstrained model-parameters, the initial value of the direct effect of friction and the reference shear stressing rate. In particular, this application shows that a decreasing stressing-rate is effective in damping the seismicity rate.

1. Introduction

Two intense episodes of surface uplift without culminating eruptions were observed in Campi Flegrei caldera near Naples (Italy; see Fig. 1) in recent times. These episodes of caldera unrest, also called bradyseisms, occurred from 1969 to 1972 and from mid-1982 to December 1984, each generating maximum uplifts of about 1.8 m (Berrino, 1998). Both uplifts were followed by a slow subsidence; in particular, some mini-uplift episodes are superimposed on that following the 1982–1984 uplift (Fig. 2a). Swarms of earthquakes correspond to episodes of fast uplift in the Campi Flegrei region (Troise et al., 2003). Berrino and Gasparini (1995) note a correlation of seismic activity with the rate of ground upheaval during unrest episodes occurred both at Campi Flegrei unrest and Rabaul volcanoes. They also suggest that on explosive volcanoes, ground deformation often precedes the onset of seismicity.

In Fig. 2b we show histories of surface displacement rate, $V(t)$, and seismicity rate, $R(t)$, observed at Campi Flegrei. The displacement rate has been computed by tide-gauge data collected at Pozzuoli harbour (Fig. 1). At that time tide-gauges were the only permanent stations which allowed monitoring the vertical ground movements continuously. The Pozzuoli instrument was the tide-gauge closest to the area where the maximum vertical movement occurs (see Fig. 1) and was located in an area where the vertical movements are about 91% of the maximum vertical movement (Berrino, 1998), so that the maximum uplift here recorded was about 1.6 m (Fig. 2a). Seismic data during the 1982–1984 unrest were recorded by 22 seismic stations on a permanent (land-based) network in the Campi Flegrei area. The seismic activity was mostly concentrated in the area between the Pozzuoli harbour, and the Solfatara crater (box in Fig. 1), that corresponds to the area where the largest uplift occurred. Seismic events with the largest magnitude were mainly located in the Solfatara area. The (minor) population of events beneath the Gulf of Pozzuoli has less constrained hypocenters owing to the open geometry of the network. We here consider a range of magnitude equal to 0.2–4.2 that corresponds to

* Corresponding author.
E-mail address: mariaelina.belardinelli@unibo.it (M.E. Belardinelli).

0012-821X/$ – see front matter © 2010 Elsevier B.V. All rights reserved.
doi:10.1016/j.epsl.2010.12.015

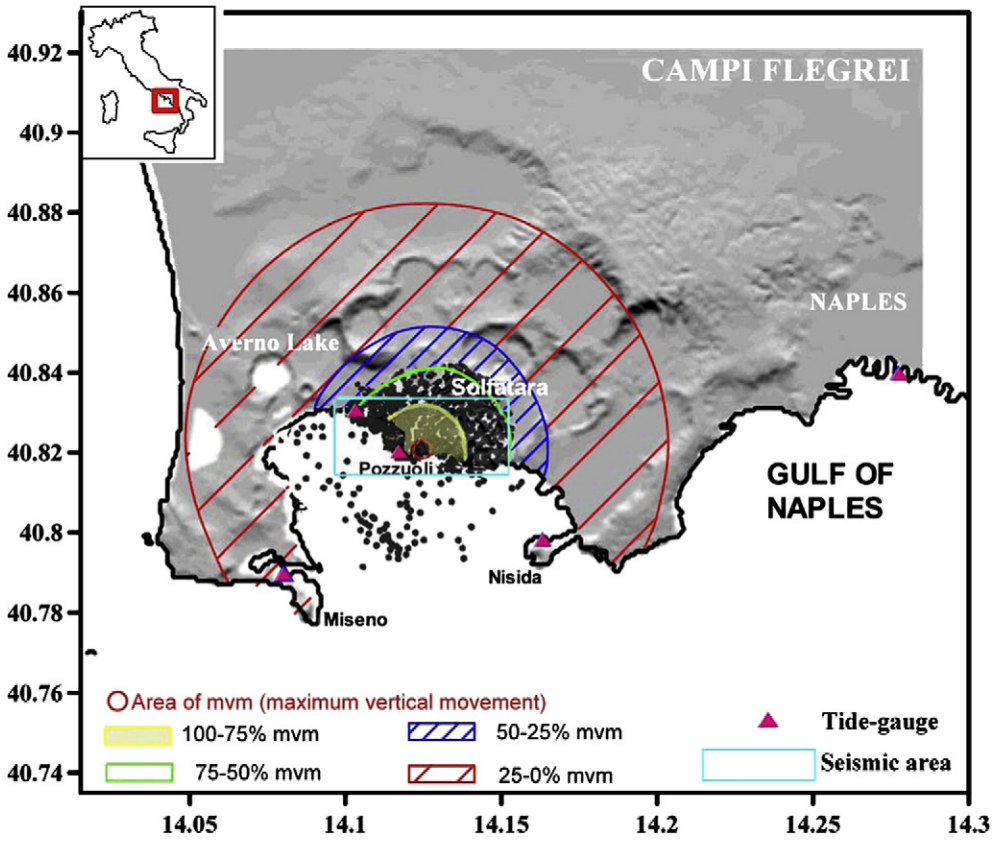

Fig. 1. Digital elevation model of Campi Flegrei area and sketch of the areal pattern of the vertical deformation. The area is divided in 4 sub-areas that are represented by the percentage of the maximum vertical movements calculated by the whole levelling data set available from 1969 to 1986. The box denoted as "Seismic area" encloses the region where the 80% of the 1982–84 seismic activity occurred. The location of tide-gauges is also shown. After Berrino (1998, modified).

events recorded by at least three stations of the seismic network in the period 1982–1984.

In this work we aim to investigate the link between uplift rate and seismicity rate during the 1982–1984 unrest episode, for which a more accurate and complete data set compared to the previous episode is available. Seismicity rates near a deformation source are often referred to stress changes induced by the same source in the surrounding region (e.g. Toda et al., 2002). First, we evaluate static stress changes caused by the inflating source. Then we translate them into stress changes as a function of time, by considering the uplift history at Campi Flegrei during the 1982–1984 unrest. Finally, we translate stressing histories into seismicity rate as a function of time by following the approach indicated by Dieterich (1994; D94 hereinafter). Table S1 of the Supplementary material lists the symbols used in this study and their definition.

2. Static stress changes

We compute static stress changes caused by an inflating source in a layered half-space, by means of a code from Wang et al. (2006). The parameters of the 1-D crustal structure assumed here are reported in Table 1. The inflating source is modeled as a penny-shaped spheroid located near Pozzuoli at 4.8 km depth with vertical inflation (aligned along the smallest axis of the spheroid). We approximate this source with a squared tensile dislocation in a horizontal plane with a 1.73 km side length. The other parameters of the source geometry here considered were inferred by previous studies from inversion of geodetic data during 1982–1984 unrest, with the same crustal model here assumed in the case of a small dimension of the source relative to its depth (Amoruso et al., 2008, their Fig. 5, solid line). Stress changes are evaluated at 2.5 km depth, that is the average depth of the $M_l \geq 3.5$ seismicity occurred near the Solfatara crater during the 1982–1984 unrest (Orsi et al., 1999). We also assume that a compressive stress is positive. In each point of a horizontal map, the changes in normal and shear stress are evaluated on optimally oriented planes for shear failure. We take into account a regional stress field present in the region before the unrest episode, that will be also referred as pre-stress. The latter is decomposed into an isotropic lithostatic stress and a homogeneous stress of tectonic origin. By taking into account that, for equilibrium reasons, near the Earth surface one of the principal axes of the pre-stress is vertical and the related principal stress should be equal to the lithostatic pressure, the principal values of the stress field of tectonic origin can be parameterized as it follows:

$$\begin{aligned} \sigma^1 &= 0 \\ \sigma^2 &= -\upsilon\sigma^T \\ \sigma^3 &= -\sigma^T. \end{aligned} \tag{1}$$

In the previous equations the principal axis 1 is vertical, $\sigma^T > 0$ for an extensional tectonics, υ is the Poisson ratio and a plain strain configuration with translational invariance along the 2-nd principal axis is assumed. Given a particular fault plane, we will indicate with τ_r and σ_r the shear and normal components of the traction, respectively, that are associated to the stress field of Eq. (1). Similarly, we will indicate with $\Delta\tau$ and $\Delta\sigma$ the corresponding components of the traction change due to the deformation source. Taking into account the effect of the deformation source causing static uplift, the total Coulomb stress acting on a fault plane can be expressed as

$$\sigma_C = \tau_r - \mu\sigma^0_{eff} + \Delta\tau - \mu\Delta\sigma \tag{2}$$

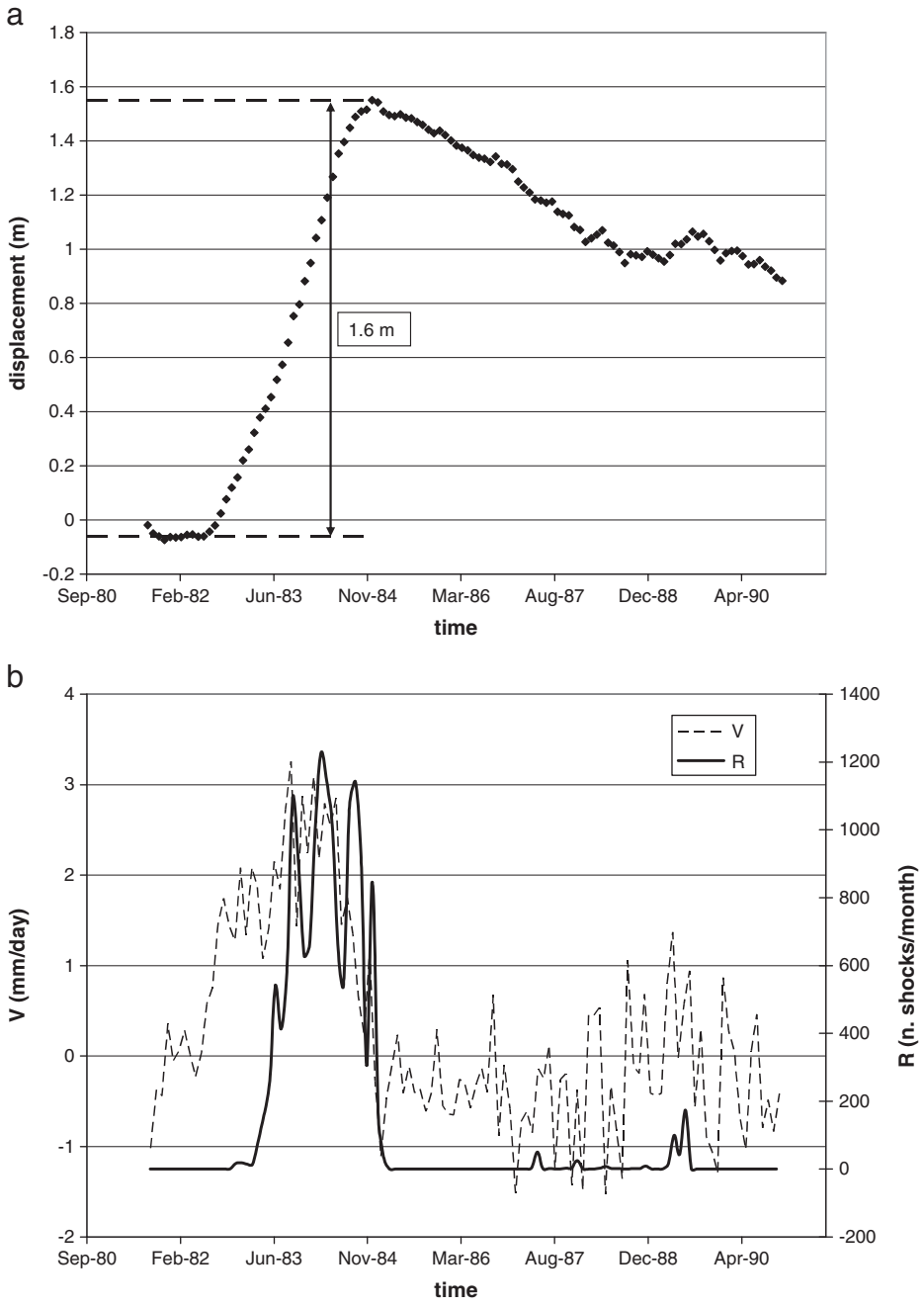

Fig. 2. 1982–84 unrest episodes and following subsidence up to 1990 in the Campi Flegrei caldera. (a) Vertical displacement (average values over 30 days) as a function of time according to a tide-gauge in the Pozzuoli harbour. (b) Seismicity rate ($R(t)$) as a function of time together with displacement rate ($V(t)$) deduced from (a). Seismicity rate data are referred to events occurred within the box shown in Fig. 1.

Table 1
Crustal model used to evaluate the static stress changes (Amoruso et al., 2008, their model A). The medium is assumed to be Poissonian (i.e., $V_P = \sqrt{3}\,V_S$, V_P and V_S being the P and S wave velocity, respectively).

Layer Top depth (km)	V_P (km/s)	Density (kg/m^3)
0	1.6	1800
0.62	2.5	2100
1.4	3.2	2270
1.55	3.9	2380
2.73	3.95	2400
3.92	5.2	2580
4.03	5.92	2700

where μ is the coefficient of friction and σ^0_{eff} is the effective normal pre-stress. The latter can be expressed as

$$\sigma^0_{eff} = \sigma_r + p_{lit} - p_f. \quad (3)$$

where p_{lit} and p_f are the lithostatic and pore fluid pressures, respectively. For the sake of simplicity, in Eq. (2) we neglect the pore fluid pressure change caused by the inflating source.

In order to constrain the least principal pre-stress direction (T-axis), we consider the analysis of focal mechanisms of the 1982–1984 crisis at Campi Flegrei made by Zuppetta and Sava (1991) where a NNE (N12°) extensional tectonics was identified in good agreement with recent results (Satriano et al., 2009). Then in the

remainder of this paper we assume that $\sigma^T>0$ and the axis 3 in Eq. (1) (T-axis) is N12° trending.

In order to constrain the value of σ^T in Eq. (1), we impose that at the onset of the 1982–1984 uplift, the shear stress acting on potential faults is comparable to, but less than, the frictional resistance $\mu\sigma^0_{eff}$. In other words, we assume that the region is in a critical state, according to the Coulomb failure criterion, just before the unrest episode. If we put in Eq. (2) $\Delta\tau=\Delta\sigma=0$ and we consider potential faults that are pure normal faults with dip angle $\delta=\frac{1}{2}\left(\pi-\arctan\left(\frac{1}{\mu}\right)\right)$ and a strike direction parallel to the principal axis relative to σ^2 (i.e., optimally oriented planes with respect to the pre-stress), then the condition $\tau_r=\mu\sigma^0_{eff}$ is equivalent to $\sigma^T=\sigma_A$, with

$$\sigma_A \equiv 2\left(p_{lit}-p_f\right)\mu\sqrt{1+\mu^2}\,/\left(1+\mu^2+\mu\sqrt{1+\mu^2}\right). \quad (4)$$

Moreover, for $\sigma^T<\sigma^A$ we have: $\tau_r<\mu\sigma^0_{eff}$.

At the depth h we can estimate $p_{lit}-p_f$ through the following relation:

$$p_{lit}-p_f = g\int_0^h (\rho(z)-\rho_w)dz \quad (5)$$

where p_f is assumed as hydrostatic, $\rho(z)$ is the rock density at depth z and $\rho_w=1000\,\mathrm{kg/m^3}$ is the water density. Considering the parameters listed on Table 1, we have $p_{lit}-p_f\cong 28.0$ MPa at the depth of 2.5 km. Moreover, for $\mu=0.85$, from Eq. (4) we have that $\sigma_A=22.0$ MPa. In the remainder of this paper we assume a regional stress characterized by $\sigma^T=18$ MPa, which is a value comparable with σ_A, but smaller than it. With this value of σ^T we can explain why seismicity was basically observed at Campi Flegrei only during the caldera unrest, that is in only in the presence of the stress perturbation created by the deformation source.

Theoretically (e.g. Anderson, 1905), in each location where stress changes are evaluated, there is a couple of optimally oriented planes for shear failure, where σ_C has the same maximum value (i.e., the stress-conjugate planes). Stress-conjugate planes are not orthogonal and they form an acute angle β related to the friction coefficient via $\tan\beta=1/\mu$. We numerically determine stress-conjugate planes by a adopting a grid-searching approach and solving for the fault planes where σ_C (expressed as in Eq. (2)) assumes the maximum value under the constraint: $\tan\beta\geq 1/\mu$. In particular, we use increments of one degree in trial values of strike, dip and rake.

In Figs. 3 and 4 we show the maps of static stress evaluated on optimally oriented planes for $\mu=0.85$, $\upsilon=0.25$ and $\sigma^T=18$ MPa.

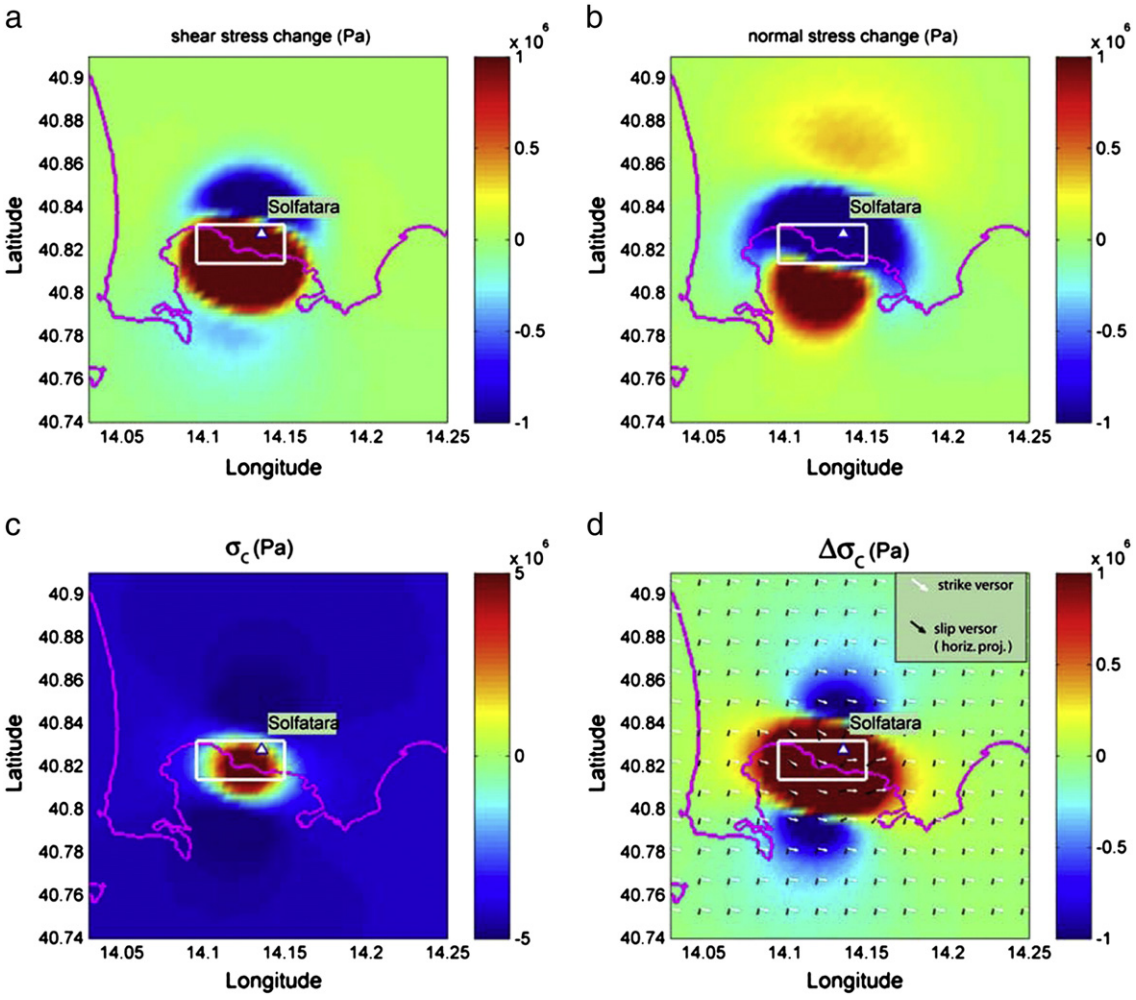

Fig. 3. Stress patterns near the deformation source responsible of the 1982–1984 unrest episode at Campi Flegrei, evaluated at a depth of 2.5 km. In each location static stresses are computed on one of the two optimally oriented planes for shear failure. The selected plane is chosen as the plane of the couple that differs less in orientation from the planes estimated in the neighboring locations. Changes in shear stress $\Delta\tau$ and normal stress $\Delta\sigma$ caused by the deformation source are represented in panels (a) and (b), respectively. In panel (c) we show the total stress of Coulomb σ_C (see Eq. (2)). In panel (d) we show the Coulomb stress change $\Delta\sigma_C=\Delta\tau-\mu\Delta\sigma$ together with the fault mechanism of the chosen plane. Black arrows represent the horizontal projection of the slip versor. White arrows represent the strike versor. The white box encloses 80% of seismicity observed during the unrest episode here studied. The magenta line represents the coast contour.

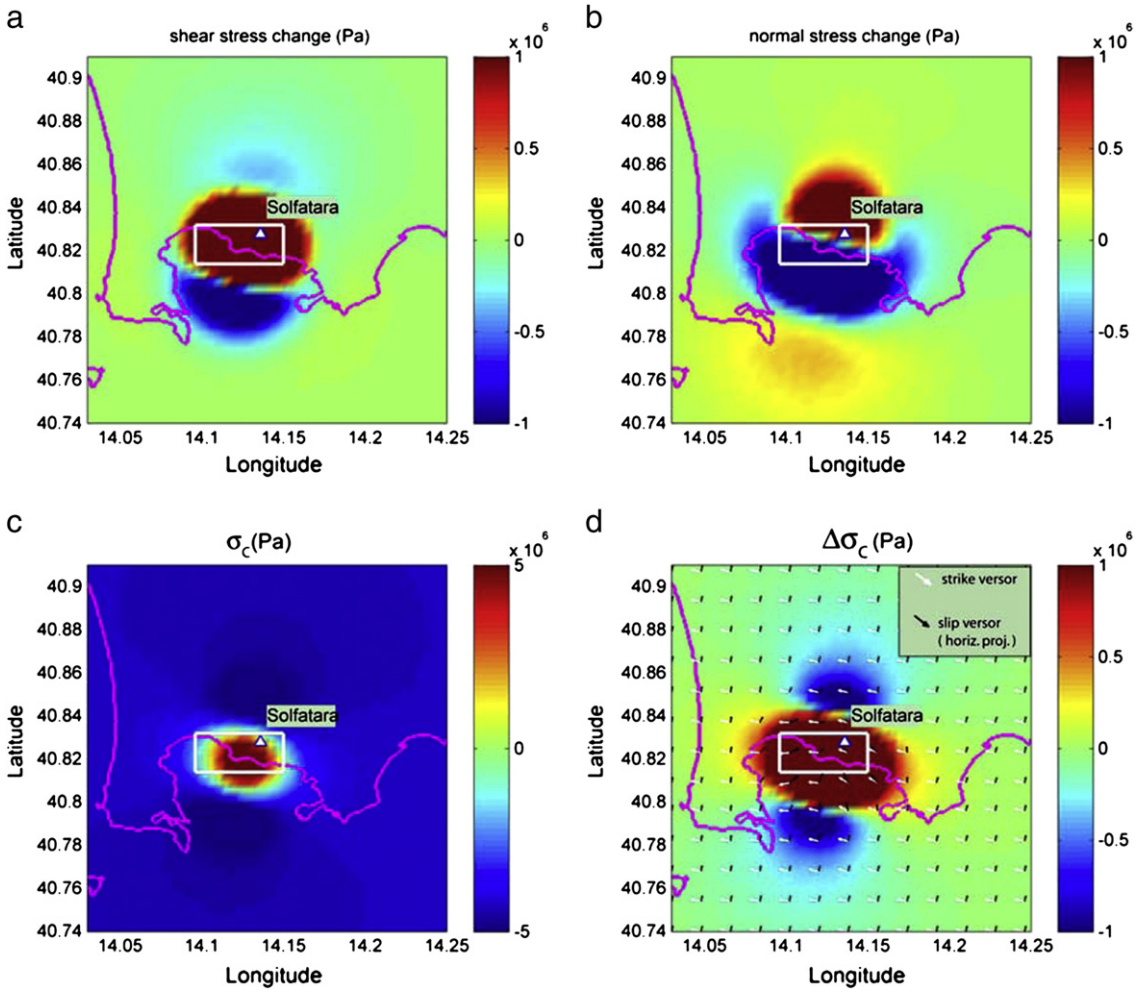

Fig. 4. The same as Fig. 3, but now for the stress-conjugate plane in the couple of optimally oriented planes.

More specifically, we show the changes in shear stress $\Delta\tau$ (panel a), normal stress $\Delta\sigma$ (panel b) and the total Coulomb stress after the deformation σ_C (panel c). In each location of the maps we plot a stress component evaluated on one plane of the couple of stress-conjugate planes, whose orientation is shown in panel d of Figs. 3 and 4. Coulomb stress changes, expressed as $\Delta\sigma_C = \Delta\tau - \mu\Delta\sigma$, are reported in Figs. 3d and 4d.

Interestingly, we can note from Figs. 3c and 4c that the region interested by non-negative values of σ_C fits with the region where most (~80%) of the seismicity observed in 1982–1984 unrest concentrates (white box in Figs. 3 and 4). This result further corroborates our choice of the tectonic stress intensity σ^T. The region where $\sigma_C > 0$ shrinks by decreasing the value of σ^T and it vanishes for $\sigma^T \leq 9$ MPa. Differences in σ_C on stress-conjugate planes as determined numerically can be referred to the discrete grid used to search the same planes. However they are less than 10 kPa, so that they cannot be appreciated in Figs. 3c and 4c.

We find that the area affected by the largest Coulomb stress changes $\Delta\sigma_C$ (dark red area in Figs. 3d and 4d) is elliptical, in agreement with the observed distribution of earthquakes during the 1982–1984 unrest (Aster and Meyer, 1988). Our results also indicate that inverse slip over the source is discouraged by the assumed regional stress, so that fault mechanisms are mostly normal with oblique components near the source and this is in agreement with observations of the 1982–1984 Campi Flegrei swarms (e.g. Troise et al., 2003). We obtain optimally oriented planes with thrust mechanisms over the inflating source only decreasing the amplitude of regional stress with respect to the value here assumed. These results are in agreement with previous studies of stress changes induced by volcanic sources in homogeneous half-spaces (Feuillet et al., 2004).

The Coulomb failure criterion suggests that, if all fault orientations have the same a priori probability to produce an earthquake, the comparison between stress-conjugate planes and the couple of nodal planes of a focal mechanism allows to choose the nodal plane where the rupture actually occurred as that one which is the closest to an optimally oriented plane, as evaluated in the hypocentral location. We recall here that it is not possible that both the nodal planes are close to one of the stress-conjugate planes, because nodal planes are orthogonal, unlike stress-conjugate planes. We perform such a kind of comparison between the couple of nodal planes and stress-conjugate planes, in the case of 16 events occurred during the 1982–1984 unrest at Campi Flegrei, with epicenters located on land and magnitudes $M_l \geq 3.5$ (Orsi et al., 1999). Stress-conjugate planes are computed at 2.5 km depth, the average depth of the 16 events, in their epicentral locations and assuming the same parameters used for Figs. 3 and 4. By indicating strike, dip and rake with ϕ_n, δ_n and λ_n for a nodal plane, and ϕ_s, δ_s and λ_s for a stress conjugate plane, for each seismic event, we choose the nodal plane which is the closest to a stress-conjugate plane by minimizing a misfit function of the angle difference:

$$\varepsilon = (\phi_n - \phi_s)^2 / \Delta\phi^2 + (\delta_n - \delta_s)^2 / \Delta\delta^2 + (\lambda_n - \lambda_s)^2 / \Delta\lambda^2 \quad (6)$$

where $\Delta\phi$, $\Delta\delta$ and $\Delta\lambda$ are twice the uncertainties in the angles of a fault plane. We tentatively estimate $\Delta\phi=40°$, $\Delta\delta=30°$ and $\Delta\lambda=40°$ by considering the widths of the 90% projection probability distribution of the composite mechanisms for 1984 earthquakes located close to the Solfatara crater (De Natale et al., 1995, their Fig. 10a). In 9 out of 16 cases, we obtain $\varepsilon<3$, indicating a general agreement within the uncertainties. In particular, for each of the two $M_l\geq4$ events whose focal mechanism and hypocentral depth are likely to be the best constrained we find $\varepsilon<0.75$. For these two seismic events the parameters of the nodal plane which is the closest to a stress-conjugate plane are listed in Table S2 of the Supplementary material, where also the nearest stress-conjugate plane is reported. We believe that these results corroborate our choices about the stress field of tectonic origin.

3. Stressing history

For simplicity, we model the average values of time dependent shear stress τ and effective normal stress σ_{eff} acting on optimally oriented planes that are located within the region where most of the recorded seismicity took place (white box in Figs. 3 and 4, hereinafter called "region of interest") during the 1982–1984 unrest. In order to determine $\tau(t)$ and $\sigma_{eff}(t)$ we refer to the static stress changes evaluated in the previous section and the observed uplift history (Fig. 2a).

From Figs. 3a, b, 4a and b we can note that there are two main kinds of stress configurations within the region of interest. In the first configuration ("PN" henceforth) the shear stress changes are positive and the changes in normal stress are negative. In the second configuration ("PP" henceforth) both shear and normal-stress changes are positive. In Table 2 we show the percentages of locations in the region of interest that are characterized by PN and PP stress configurations in the case of Figs. 3 and 4. From Figs. 3a, b, 4a and b it emerges that if we compute the mean change in normal stress acting on a couple of stress-conjugate planes located within the region of interest or, for each plane in the couple, we average the change in normal stress within the region of interest (at least in the case of Fig. 4), we obtain a much smaller value than the correspondent change in shear stress. In order to obtain an average change in normal stress that is comparable in absolute value with that in shear stress, we average stress changes by keeping separate the PP and PN configurations. For both configurations, we evaluate the average components of stress changes and pre-stress in the case of Figs. 3 and 4. Results are reported in Table 2. For each stress configuration, we then consider mean values among Figs. 3 and 4 obtaining the values listed in the first four rows of Table 3.

In Fig. 2a we show the averaged data of uplift that were recorded by a tide-gauge located in Pozzuoli at Campi Flegrei. Each datum is the average of daily uplift over an interval lasting 30 days and it is referred to the 15-th day of the interval. We normalize these observations to the maximum increment of uplift with respect to January 1982, which amounts to about 1.6 m (see Fig. 2a). The history of normalized displacement obtained in this way is then approximated with a piecewise-linear function that we denote as $f(t)$. We assume intervals lasting 30 days of constant displacement rate.

Table 2
Parameters characterizing the PN and PP configuration in case of Figs. 3 and 4 (percentage of occurrences in the region of interest and average values of stress components in that region).

Parameter	Configuration PN		Configuration PP	
	Fig. 3	Fig. 4	Fig. 3	Fig. 4
%	93.3	68.3	6.7	31.7
$\Delta\tau$ (MPa)	5.55	7.08	5.66	8.30
$\Delta\sigma$ (MPa)	−2.89	−1.51	0.07	0.87
τ_r(MPa)	7.24	6.16	4.72	3.01
σ^0_{eff}(MPa)	14.70	12.93	11.52	10.66

Table 3
First four rows: parameters used to describe the time histories of shear and normal stress (see Eq. (7)). For each configuration and parameter, the mean value between results of Figs. 3 and 4 (see Table 2) is reported. Last two rows: preferred values of the parameters of the seismicity rate model in comparison with data.

Parameter	Configuration PN	Configuration PP
$\Delta\tau$ (MPa)	6.32	6.98
$\Delta\sigma$ (MPa)	−2.20	0.47
τ_r(MPa)	6.70	3.86
σ^0_{eff}(MPa)	13.82	11.09
A_0(MPa)	0.225	0.260
$\dot{\tau}_r$(MPa/yr)	8.4×10^{-4}	9.1×10^{-4}

We attribute the same normalized temporal dependence, $f(t)$, to both τ and σ_{eff}. In so doing we assume that $f(t)$ is due mainly to time-dependent processes occurring at the inflating source. A similar assumption was made by Toda et al. (2002) for the analysis of the seismicity induced by a dyke intrusion. Specifically we assume:

$$\tau(t)=\begin{cases}\tau_r+\dot{\tau}_r(t-t_0), & t_0\leq t<t_1\\ \tau_r+\dot{\tau}_r(t-t_0)+f(t)\Delta\tau, & t\geq t_1\end{cases}$$
$$\sigma_{eff}(t)=\begin{cases}\sigma^0_{eff}, & t_0\leq t<t_1\\ \sigma^0_{eff}+f(t)\Delta\sigma, & t\geq t_1\end{cases} \quad (7)$$

where $\dot{\tau}_r$ is the reference shear stressing rate in the Campi Flegrei region, $t=t_0$ correspond to August, 3, 1981 (i.e., the beginning of the record of displacement) and $t_1-t_0=15$ days. Values of other parameters in Eq. (7) are listed in the first four rows of Table 3 for the PN and PP configuration. By construction, the stressing histories $\tau(t)$ and $\sigma_{eff}(t)$ obtained in this way are piecewise-linear functions of time, in that the stressing rates $\dot{\tau}$ and $\dot{\sigma}_{eff}$ are constant during each interval lasting 30 days within the time window reported in Fig. 2.

4. Seismicity rate-changes

According to the D94 approach, the stressing history controls the timing of earthquakes on a fault population obeying to a rate- and state-dependent rheology. The latter is represented by laboratory-derived friction laws, that express the frictional resistance on the sliding surfaces as a function of the slip velocity and a state variable, accounting for previous slip episodes (e.g., Ruina, 1983 and references cited therein). In particular, the time-dependent seismicity rate $R(t)$ can be expressed as (Eq. (11) in D94):

$$R=\frac{r}{\gamma\dot{\tau}_r} \quad (8)$$

where $\dot{\tau}_r$ is the reference shear stressing rate, r is the reference (or background) seismicity rate and $\gamma(t)$ ($[\gamma]=$s/Pa) is a state variable representing the dependence of R on the stressing history. The state variable γ evolves through time according to the following non-linear, first-order, ordinary differential equation (cfr. Eq. (9) in D94):

$$\dot{\gamma}=\frac{1}{a\sigma_{eff}}\left[1-\gamma\dot{\tau}+\gamma\left(\frac{\tau}{\sigma_{eff}}-\alpha\right)\dot{\sigma}_{eff}\right] \quad (9)$$

where a and α are two constitutive parameters controlling the fault rheology (here assumed constant through time). In the previous equation $\dot{\tau}$ and $\dot{\sigma}_{eff}$ are time derivative of the histories of shear stress, $\tau(t)$, and normal stress, $\sigma_{eff}(t)$, respectively, applied to the fault population. The term $a\sigma_{eff}$ represents the so called direct effect on

the frictional resistance (e.g., Belardinelli et al., 2003). We indicate with $A_0 = a\sigma_{eff}^0$ the initial (i.e. at $t = t_0$) value of the direct effect on friction according to Eq. (7). Eq. (9) can be rewritten as

$$\dot{\gamma} = \frac{1}{A_0 r_n}\left[1 - \gamma\dot{\tau} + \gamma(r_s - \alpha)\dot{\sigma}_{eff}\right] \tag{10}$$

where $r_n \equiv \sigma_{eff}/\sigma_{eff}^0$ and $r_s \equiv \tau/\sigma_{eff}$.

In this section, we translate the records of shear and effective normal stress, computed in the previous section (Eq. (7)), into seismicity rate as a function of time $R(t)$ by solving Eq. (10) and inserting the result in Eq. (8). We assume $\gamma(t = t_0) = \dot{\tau}_r^{-1}$, which corresponds to a value of R equal to the background seismicity rate r. We evaluate $R(t)$ as the number earthquakes per day and then we numerically integrate it from the beginning up to the end of each month of the considered time window in order to get $R(t)$ in terms of number of earthquakes per month. As shown in details in Appendix A, we solve Eq. (10) by considering the case of rates of shear and effective normal stresses applied to the fault population that are step functions of time. In Eq. (10), we assume $\alpha = 0.25$, a value within the experimental range (Linker and Dieterich, 1992), also considered in dynamic models of thermally pressurized fault zones (Bizzarri and Cocco, 2006). We also assume $r = 0.25$ earthquakes/month in Eq. (10) by considering the number of $M_l \geq 0.2$ earthquakes per month occurred in the region of interest in the years 2002–2004 when a benchmark located near Pozzuoli was affected by changes in elevation in intervals of six months that were significantly smaller in absolute value than in the previous deflating period 1985–2001 (e.g. Del Gaudio et al., 2010). Indeed in the period preceding the unrest episode here considered, annual levelling surveys carried out between 1975 and 1981 did not show changes in elevation larger then few centimetres (Orsi et al., 1999). On the other hand, it is not possible to evaluate r in the period preceding 1982–1984, as it is usually made in seismicity rate studies, owing to catalogue incompleteness. In our simulations we consider different values of $\dot{\tau}_r$ and A_0, the last free parameters in Eqs. (7) and (10).

Previous approaches (e.g. Catalli et al., 2008; Dieterich et al., 2000) assumed constant values for $r_n = 1$ and r_s in Eq. (10), while in general both r_n and r_s are variable with time. This is the case of the present study, in that the time-dependent stresses $\tau(t)$ and $\sigma_{eff}(t)$ expressed by Eq. (7) cause time variations of r_n and r_s appearing in Eq. (10). In order to determine $\gamma(t)$ by solving Eq. (10), we therefore consider two cases where we either consider r_n and r_s as constant (Case 1) or variable (Case 2).

In Case 1, which is analogous to previous studies, we determine $\gamma(t)$ as the solution of Eq. (10) for $r_n = 1$ and $r_s = \tau_r/\sigma_{eff}^0$, which is $r_s(t = t_0)$ according to Eq. (7). In so doing we solve

$$\dot{\gamma} = \frac{1}{A_0}\left[1 - \gamma\dot{\tau} + \gamma\left(\frac{\tau_r}{\sigma_{eff}^0} - \alpha\right)\dot{\sigma}_{eff}\right]. \tag{11}$$

where only $\dot{\tau}(t)$ and $\dot{\sigma}_{eff}(t)$ are variable as step functions of time.

In Case 2 we determine $\gamma(t)$ as the solution of an approximation of Eq. (10) where we consider $r_n(t) = \sigma_{eff}(t)/\sigma_{eff}^0$ and $r_s(t) \equiv \tau(t)/\sigma_{eff}(t)$ with $\tau(t)$ and $\sigma_{eff}(t)$ that are piecewise-linear functions of time according to Eq. (7). The second member of Eq. (10) is approximated in each interval of constant stressing rate by considering only first-order variations of $\tau(t)$ and $\sigma_{eff}(t)$ relative to the values at the beginning of the interval. Analytical details about the solutions of Case 1 and Case 2 are reported in Appendix A.

A comparison between the two cases is reported in Fig. 5, for the same stressing history and the same values of A_0 and $\dot{\tau}_r$ that are chosen in order to reproduce the observed data of seismicity using the Case 2 solution, as we will see in the remainder of this section. It is interesting to note that the Case 1 solution with the PN stress configuration underestimates the observed amplitudes while it provides a slight overestimate of data if the PP stress configuration is considered. This can be explained as it follows. In Case 1 we assume a constant value of $a\sigma_{eff} = A_0$, while in Case 2 the time variation of $a\sigma_{eff}(t) = A_0 r_n(t)$ causes a decrease (increase) of $a\sigma_{eff}(t)$ starting from A_0 that in turn produces an unclamping (clamping) effect to the fault population subjected to the PN (PP) stress configuration. However, the effect is smaller for the PP stress configuration where a smaller value of the ratio $|\Delta\sigma|/\sigma_{eff}^0$ is present than in the PN case (Table 3). In the remainder of this section the seismicity rate as a function of time is computed by considering Case 2, unless otherwise specified.

The dependence of the model on the values of A_0 and $\dot{\tau}_r$ is summarized in Fig. 6 for the PN stress configuration obtained in the previous section. Parameters A_0 and $\dot{\tau}_r$ mostly affect the temporal dependence and the amplitudes of $R(t)$, respectively. An increase in the parameter A_0 entails a larger time scale. On the other hand, increasing $\dot{\tau}_r$ produces smaller values of $R(t)$.

The results of our preferred model compared with the observed rates of seismicity are shown in Fig. 7 for PN and PP stress configurations. Both configurations are characterized by similar values of parameters A_0 and $\dot{\tau}_r$, as reported in Table 3, that are chosen in order to reproduce the initial stage of the observed rate of seismicity as a function of time, i.e. its onset in the period December 1982–May 1983 (Fig. 7) and the amplitude of its second peak (September 1983).

In the period 1982–1984 we can see that the model can reproduce the largest amplitudes of seismicity rate, even if several observed maxima correspond to inflection points in the model. Unlike data, the model predicts a maximum value of $R(t)$, closely following a peak of displacement rate in May 1984 (Fig. 7). However, there is a good agreement between model and observations in the period March–April 1984 (a large swarm with hundreds of shocks occurred at April the first 1984). The return to values comparable with the background seismicity rate at the end of the 1982–1984 unrest is present in model results of Fig. 7 even if it is delayed with respect to observations. In general, the values of $R(t)$ following peaks are overestimated by the present model. Finally from Fig. 5 we can also see that the model fails to predict small swarms subsequent to the 1982–1984 unrest, as we will discuss in the following section.

5. Discussion and concluding remarks

In this paper we model the seismicity observed during 1982–1984 unrest at Campi Flegrei. To this goal we compute the stress changes caused by the source responsible of the observed vertical ground displacement (deformation source). Static changes of stress are spatially averaged and transformed into time-dependent components of stress, by taking into account the observed history of ground displacement. Seismicity rate changes are then estimated according to the D94 approach (see Eq. (8)).

Static stress–changes due to the deformation source associated to the Campi Flegrei unrest are evaluated on optimally oriented planes for shear failure by assuming an extensional stress field of tectonic origin whose magnitude is constrained by imposing that the initial state of the region (in the absence of the stress perturbations caused by the deformation source) is “close to failure”, according to the Coulomb failure criterion. With this constraint, when the effect of the deformation source is taken into account, the total stress of Coulomb is positive in a region that correlates with the here-called region of interest (white box in Figs. 3 and 4), where most of 1982–1984 seismicity was observed.

An outcome of the present study is that we find that optimally oriented planes generally represent normal faults with oblique components above the inflating source; this is in agreement with observations (e.g. Orsi et al., 1999). For the two largest shocks ($M_l \geq 4$) we find a good agreement between one of the stress-conjugate plane evaluated in the location of the shocks and a nodal plane of the focal mechanism (Table S2 of the Supplementary material). In the region of

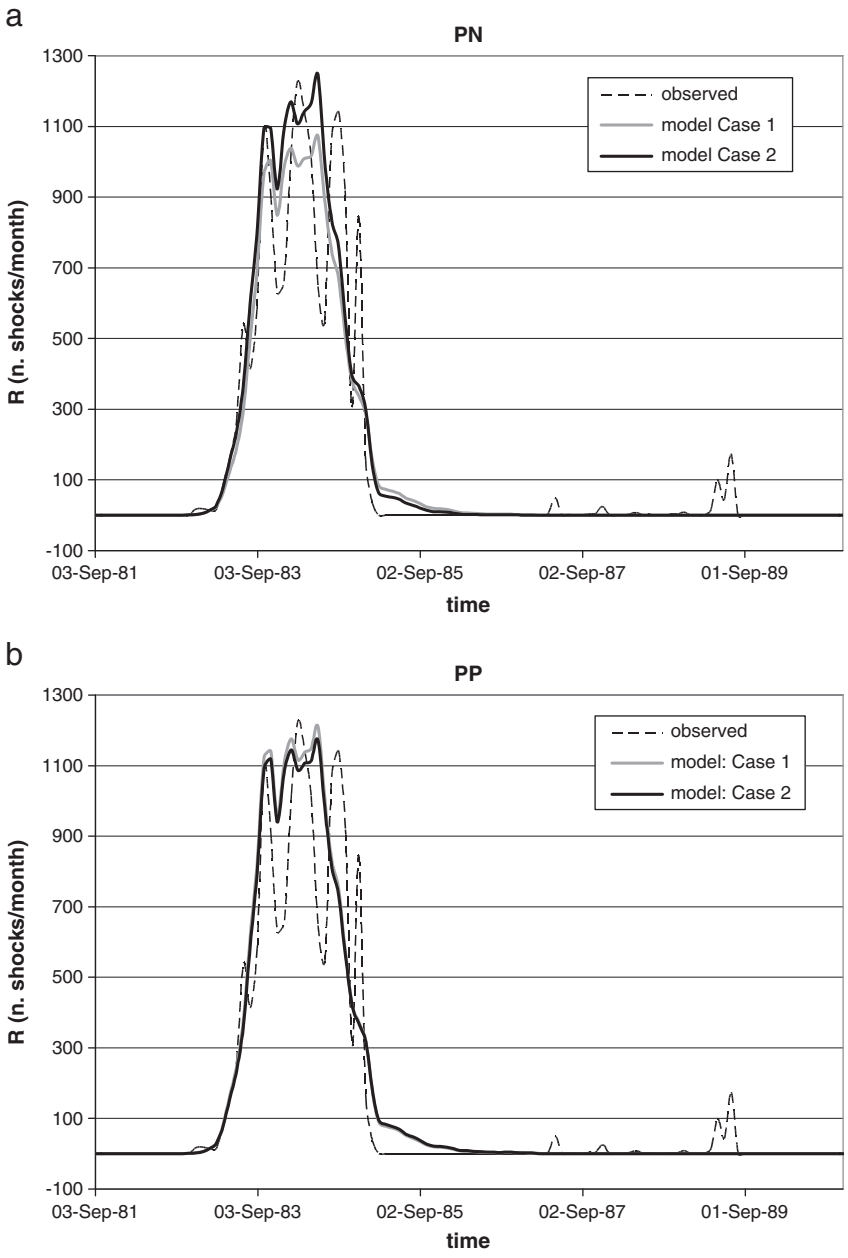

Fig. 5. Comparison between results obtained following the two approximated methods to estimate $R(t)$, see Section 4 for explanation: Case 1 (gray solid line) and Case 2 (black solid line). Data are represented by the black dashed line. In panel (a) we show the results for the PN stress configuration (see Section 3 for details) with $A_0 = 0.23$ MPa, $\dot{\tau}_r = 8.4 \times 10^{-4}$ MPa/yr. In panel (b) we show the results for the PP stress configuration (see Section 3 for details) with $A_0 = 0.26$ MPa and $\dot{\tau}_r = 9.1 \times 10^{-4}$ MPa/yr. In Case 2 of panel (b) during inflation time intervals ($V(t) > 0$), we determine $R(t)$ by using the solution (A8) where the integrand is expanded in Taylor series in t up to the eight order. (This is due to numerical problems preventing the use of the explicit solution, first equation of Eq. (A9)).

interest, there are two main configurations of stress with positive values of shear and normal components of opposite sign. In order to evaluate the effect of changes in normal stress, we keep separate the two configurations of stress, without averaging between them.

The present model focuses on the temporal evolution of the seismicity rate at Campi Flegrei. The case of 1982–1984 unrest shows that uplift rates with a long time scale (compared to coseismic ones) precede and accompany the seismicity rate (Figs. 2 and 7). In the literature the effect of increasing stressing rates on seismicity has been often remarked, while in the present model at the end of uplift and during the subsequent subsidence stressing rates useful for Coulomb failure are decreasing and negative, respectively. The effect of this kind of stressing rates in damping the seismic activity is here particularly evident (Fig. 7).

Compared to previous applications to volcanic areas, that considered a piecewise-constant approximation of shear and normal stress as a function of time (e.g. Dieterich et al., 2000), we assume here a piecewise-linear approximation of them. In order to model the seismicity rate as a function of time, we consider time intervals of constant rates of shear and effective normal stress. In each interval we solve two approximated equations for the evolving part of the seismicity rate: Case 1 and Case 2. The comparison between results in the two cases (Fig. 5) shows that the time variations of $A_0 r_n(t) = a\sigma_{eff}(t)$ and $r_s(t) = \tau(t)/\sigma_{eff}(t)$ in Eq. (10), that are considered in Case 2, unlike Case 1, can affect seismicity rate amplitudes (Fig. 7a). This is the case if a change in normal stress with relatively large amplitude compared to the initial effective normal stress is applied to a fault population, as it is in the PN stress configuration (Fig. 5a).

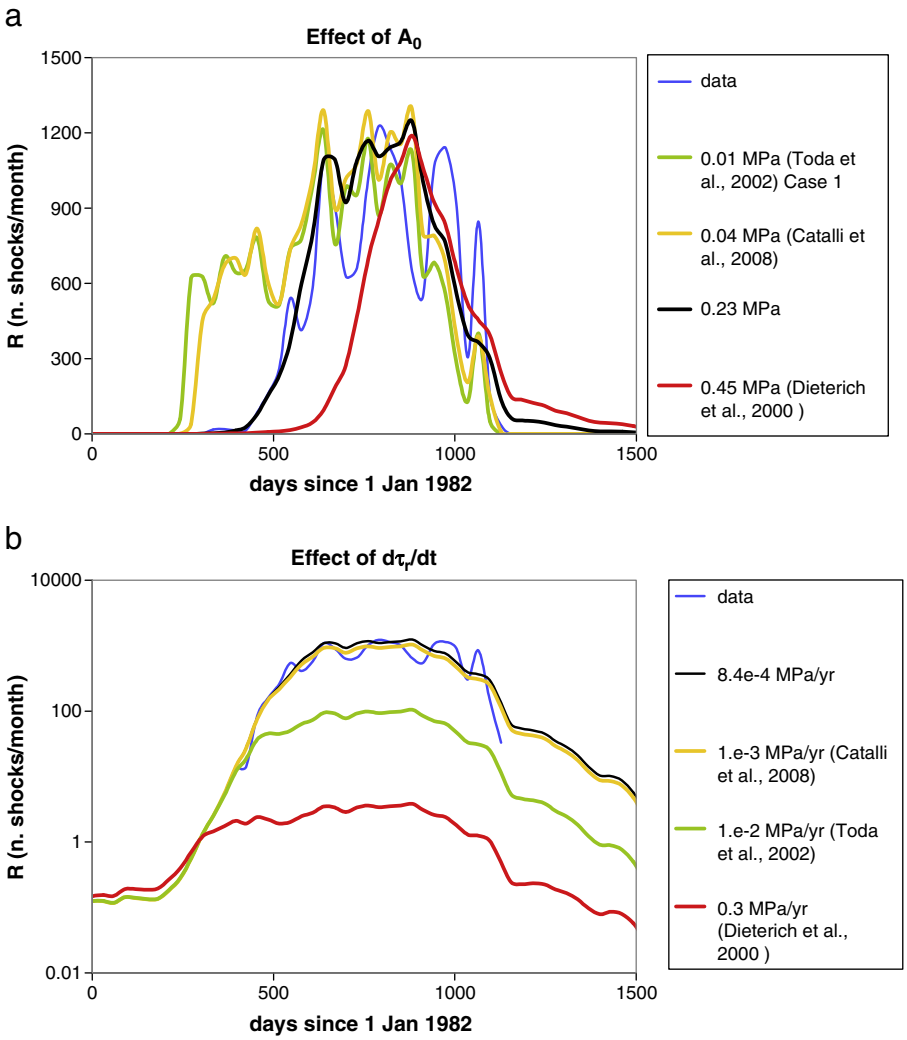

Fig. 6. Effect of parameter variation in the case of the PN configuration. (a) Effect of different values of A_0, leaving $\dot{\tau}_r = 8.4\times10^{-4}$ MPa/yr. (b) Effect of different values of $\dot{\tau}_r$, leaving $A_0 = 0.23$ MPa (as in Fig. 5a). The black curve represents the preferred value of the parameter varied in each panel, on the basis of the comparison of the present model with seismicity rate data (blue line). We also consider some other values of parameters taken from the literature: they were assumed (Dieterich et al., 2000, red line, Toda et al., 2002, green line) or inferred (Catalli et al., 2008, yellow line) in models based on the D94 approach for seismicity rate estimates. In the case with $A_0 = 0.01$ MPa in panel (a) we are able to compute $R(t)$ only in Case 1 (see text for details). In the case with $\dot{\tau}_r = 0.3$ MPa/yr in panel (b), during deflation time intervals ($V(t)<0$) we use the solution (A8) where the integrand is expanded in Taylor series in t up to the eight order. Note the logarithmic scale in panel (b).

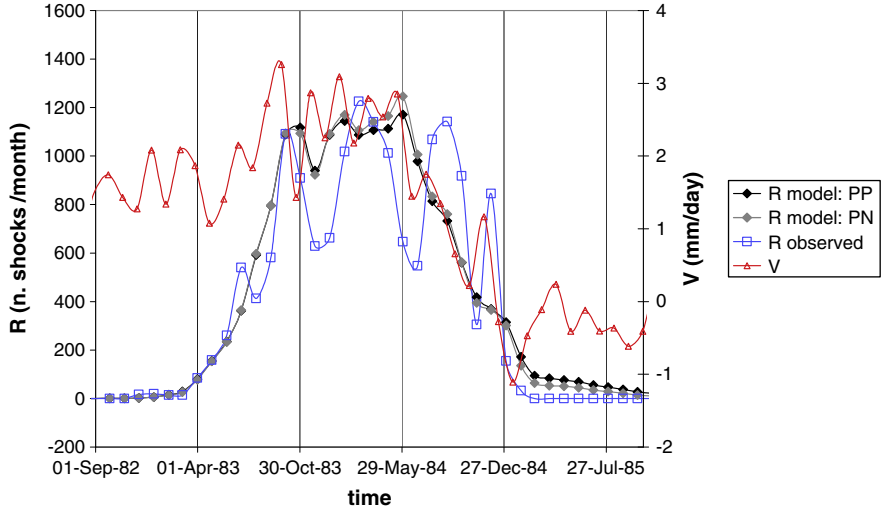

Fig. 7. Preferred model in case of the PP (black line with solid diamonds) and PN (gray line with solid diamonds) stress configurations. Parameter values are reported in Table 3. The red line represents displacement rate ($V(t)$) as a function of time (Fig. 2b) and the blue line represents seismicity rate data ($R(t)$). In the case of the PP configuration, we determine $R(t)$ during inflation time intervals ($V(t)<0$) by using the solution (A8) where the integrand is expanded in Taylor series in t up to the eight order (see also the caption of Fig. 5).

The present model is able to estimate well the maximum amplitudes and the duration of the observed rate of seismicity in the period 1982–1984 (Figs. 5–7). Seismicity rate estimates based on the approach proposed by D94 require the knowledge of the stressing rates and then the modeling of the source producing them. The failure of the present model in predicting the seismicity rate after the end of 1984 (see Fig. 5) might be explained if the sources responsible of subsequent uplifts are different from the deformation source that causes the 1982–1984 uplift (Gottsmann et al., 2003; Rinaldi et al., 2009). Subsequent minor episodes of uplift at Campi Flegrei in particular can be a consequence of hydrothermal fluid circulation in the aquifer (Gaeta et al., 2003; Gottsmann et al., 2003 and Rinaldi et al., 2009).

We propose a simplified way to obtain the stress field as a function of time, that requires the knowledge of temporal records of displacement as a function of time produced by the deformation source. Unlike the 1982–1984 unrest, at the present this kind of data could be easily provided by permanent and continuous GPS stations, that currently are present at the Campi Flegrei caldera. The short-term differences between the model results and observations in the unrest period 1982–1984 (Figs. 6 and 7) might be related to either the incompleteness of the seismic catalogue or the accuracy of the observed displacement history, which, we recall, represents a model input. In fact, the present model is strongly dependent on stressing rates or displacement rates histories. This kind of sensitivity is well known since, according to Dieterich et al. (2000), it can be even used to retrieve the stressing history from the seismicity rate as a function of time. Concerning the underestimate of the $R(t)$ fluctuation amplitude in the 1982–1984 unrest (Fig. 7), it is worth to recall that the approach followed here does not take into account the finiteness of the population of faults that are prone to failure. As discussed by Gomberg et al. (2005), this can lead to overestimates of $R(t)$ after the application of a large positive stressing rate such as that caused by a mainshock.

The present model simplifies the time dependence of the stress field because it attributes it to the deformation source only, and because, by assuming a spatially-averaged point of view, it does not take into account local effects that can affect seismicity. We also neglect the effect of eight major shocks observed during the 1982–1984 unrest ($3.8 \leq M_l \leq 4.2$). This might explain the short-term differences between our model and the recorded seismicity too. However there is not a clear evidence of aftershock sequences following most of the largest shocks recorded at Campi Flegrei during the 1982–1984 unrest. Besides this, for the Umbria–Marche seismic sequence occurred in 1997 Catalli et al. (2008) find that taking into account $3.8 \leq M_l \leq 5$ earthquakes has negligible effects on seismicity rate estimates.

In modeling the seismicity rate $R(t)$ on the basis of the D94 approach, we estimate the two unconstrained parameters ($A_0 = a\sigma^0_{eff}$ and $\dot{\tau}_r$) that allow the model to reproduce the initial part of the observed record of seismicity rate. Our estimates of unconstrained parameters are listed in the last two rows of Table 3. Uncertainties in stress modeling related to the source geometry together with the variability of the seismicity depth (that in the case of this episode of unrest at Campi Flegrei is also quite uncertain, e.g., Orsi et al., 1999) can affect our estimates of the above mentioned parameters. This is due to the fact that the estimate of A_0 increases with the amplitude of the stress change. On the other hand larger stress changes tend to produce larger amplitudes of $R(t)$ and, according to our results (Fig. 6b), they require a larger estimate of $\dot{\tau}_r$ in order to reproduce the same amplitude of $R(t)$. We verified that a 5.2 km depth of the inflating source (as suggested by Bonafede et al., 2010) leads to results for $a = A_0/\sigma^0_{eff}$ and $\dot{\tau}_r$ similar to those obtained here (with 4.8 km source depth and 2.5 km seismicity depth) provided that stress changes are evaluated at 3 km depth (the average depth of in land seismicity, e.g. Aster and Meyer, 1988). Instead, a 0.5 km decrease in the depth distance between source and seismicity, leads to larger stress changes and larger values up to 25% for $a = A_0/\sigma^0_{eff}$ and 90% for $\dot{\tau}_r$. Moreover, owing to catalogue incompleteness, the reference seismicity rate r can't be reliably evaluated in the period preceding the 1982–1984 unrest and we verified that a 100% increase of r with respect to the value here assumed leads to about the same increase of $\dot{\tau}_r$ and a 10% increase of A_0 with respect to values reported in Table 3. Therefore a previous suggestion of a correlation between the parameters that affect $R(t)$ according to the D94 approach (Cocco et al., 2010) is verified also in the present study, where a different stressing history with respect to a pure step is taken into account.

The delay of about some months of the seismic activity with respect to the beginning of uplift in the 1982–1984 unrest (Berrino and Gasparini, 1995) allows us to constrain the value of the rheological parameter A_0. By assuming the values of σ^0_{eff} and A_0 reported in Table 3, we have that the comparison of the present model with data suggests a range [0.016–0.023] for the parameter a, which encompasses values inferred from laboratory experiments. However, we notice that the upper end of this range tends to suggest hydrothermal conditions (D94). We emphasize that the interior of the Campi Flegrei unrest region is characterized by geothermal gradients that rank among the highest in the world (Gaeta et al., 2003). On the other hand, our estimate of the reference shear stressing rate $\dot{\tau}_r$ (Table 3) agrees with a value regarded as suitable for other regions of the Apennine chain (e.g. Catalli et al., 2008), even if we confirm that this parameter is strongly correlated with the background seismicity rate.

To conclude, the present application to 1982–1984 unrest episode at Campi Flegrei is encouraging for studies dealing with modeling of seismic activity for which the importance of taking into account stressing rate changes is confirmed. Our results clearly show that the seismicity rate changes can be affected by either decreasing or increasing the stressing rate in a volcanic region. Moreover, we believe that the present analysis supports the idea that, in order to explain the space–time patterns of seismicity in volcanic areas with low seismic efficiency, the deformations (stresses) varying on relatively long time scales play such a prominent role as the coseismic ones in seismogenic areas.

Acknowledgements

The authors are grateful to L. Crescentini for having provided a revised version of the code used to evaluate static stress changes in a layered half-space. We also thank P. Gasperini for the availability of FPSPACK to compute the nodal plane angles from CMT principal axes. We appreciated the detailed comments by the Editor, Y. Ricard, and by two anonymous referees that contribute to improve the paper. This work has been developed within the project UNREST, funded by the Department of Civil Protection of Italy.

Appendix A. Computation of the seismicity rate from the model of Dieterich (1994)

We solve here Eq. (10) in order to obtain the seismicity rate $R(t)$ from Eq. (8), according to the Dieterich (1994) approach (D94 henceforth). We consider the particular case of rates of shear and effective normal stresses applied to the fault population that are step functions of time. In the present application to the 1982–1984 unrest at Campi Flegrei, the time histories of shear and normal stress ($\tau(t)$ and $\sigma_{eff}(t)$, respectively) that appear in Eq. (10) are expressed as in Eq. (7). In order to approximate $\tau(t)$ and $\sigma_{eff}(t)$ in a piecewise-linear way, we divide the time window of interest into sub-intervals $t_k < t \leq t_{k+1}$ (with $k = 1, 2, \ldots$ and $t_{k+1} = t_k + \Delta t$), all lasting $\Delta t =$ 30 days, during which $\dot{\tau}$ and $\dot{\sigma}_{eff}$ can be assumed as constants, $\dot{\tau} = \dot{\tau}_k$ and $\dot{\sigma}_{eff} = \dot{\sigma}_k$. In the remainder of this appendix we will denote with symbols τ_k and σ_k the values of shear and effective

normal stress, respectively, attained at the time instant $t=t_k$ (so that $\tau(t_k)=\tau_k$ and $\sigma_{eff}(t_k)=\sigma_k$).

In order to solve Eq. (10), it is also necessary to know the value of the state variable γ at the beginning of in each interval. Let we indicate with $\gamma_k \equiv \gamma(t_k)$ and $\gamma_k^f \equiv \gamma(t_k+\Delta t)$ the values of γ at the beginning and at the end of each interval, respectively. Since $\gamma_{k+1}=\gamma_k^f$ by definition, it is possible to determine $\gamma(t)$ in the k-th interval ($k>0$) if Eq. (10) is solved in all the previous time intervals $]t_j, t_j+\Delta t]$, $j=0,\ 1,\ldots,\ k-1$.

In each sub-interval, we consider two cases where we either consider in Eq. (10) $r_n \equiv \sigma_{eff}/\sigma_{eff}^0$ and $r_s \equiv \tau/\sigma_{eff}$ as constant (Case 1) or variable (Case 2).

A.1. Case 1

As a first approximation, we assume in Eq. (10) constant values of $r_n=1$ and $r_s=\mu_0$. In this case Eq. (10) for $t_k<t\le t_k+\Delta t$ can be simplified to

$$\frac{d}{dt}\gamma = \frac{1}{A_0}[1-c_1\gamma] \tag{A1}$$

where

$$c_1 \equiv \dot{\tau}_k - (\mu_0-\alpha)\,\dot{\sigma}_k. \tag{A2}$$

The solution of Eq. (A1) is:

$$\gamma(t) = \left(\gamma_k - \frac{1}{c_1}\right)\exp\left[-\frac{c_1(t-t_k)}{A_0}\right] + \frac{1}{c_1}. \tag{A3}$$

From Eq. (A3) it is possible to obtain the solution (B17) of D94 (pertaining to the case of constant shear stressing rate), simply by imposing $\dot{\sigma}_k = 0$ in Eq. (A2).

A.2. Case 2

A second scenario we consider to solve Eq. (10) is the case of time variable r_n and r_s. By recalling the definitions of r_n and r_s and considering that $A_0 = a\sigma_{eff}^0$, we can rewrite Eq. (10) for $t_k<t\le t_k+\Delta t$ as it follows

$$\dot{\gamma} = \frac{1}{a\sigma_{eff}(t)}\left[1-\gamma\dot{\tau}_k + \gamma\left(\frac{\tau(t)}{\sigma_{eff}(t)}-\alpha\right)\dot{\sigma}_k\right] \tag{A4}$$

where we consider a linear variation of $\tau(t)$ and $\sigma_{eff}(t)$ for $t_k<t\le t_k+\Delta t$:

$$\begin{aligned}&\tau(t) = \tau_k + \delta\tau(t), \quad \delta\tau(t) \equiv \dot{\tau}_k(t-t_k)\\ &\sigma_{eff}(t) = \sigma_k + \delta\sigma(t), \quad \delta\sigma(t) \equiv \dot{\sigma}_k(t-t_k).\end{aligned} \tag{A5}$$

After substitution of Eq. (A5) into Eq. (A4) and after developing in Taylor series to the first order in $\delta\sigma/\sigma_k$ and $\delta\tau/\tau_k$ the second member of Eq. (A4), we obtain an approximate evolution equation for the state variable γ:

$$\frac{d\gamma}{dt'} = \frac{1}{a\sigma_k}[1-c_1\gamma-c_2t' + c_3t'\gamma] \tag{A6}$$

where

$$\begin{aligned}&t' \equiv t-t_k, \quad \mu_k \equiv \frac{\tau_k}{\sigma_k}\\ &c_1 \equiv \dot{\tau}_k - \dot{\sigma}_k(\mu_k-\alpha)\\ &c_2 \equiv \frac{\dot{\sigma}_k}{\sigma_k}\\ &c_3 \equiv \dot{\sigma}_k\frac{2\dot{\tau}_k - 2\mu_k\dot{\sigma}_k + \alpha\dot{\sigma}_k}{\sigma_k}.\end{aligned} \tag{A7}$$

The solution of Eq. (A7) can be written as:

$$\gamma(t') = \left[\gamma_k + \frac{1}{a\sigma_k}\int_0^{t'}(1-c_2t)\exp\left(\frac{2c_1-c_3t}{2a\sigma_k}t\right)dt\right]\exp\left(-\frac{2c_1-c_3t'}{2a\sigma_k}t'\right). \tag{A8}$$

The integral appearing in Eq. (A8) can be solved analytically in closed-form obtaining:

$$\begin{aligned}\gamma(t') = \frac{1}{|c_3|s}\Big\{&s\exp\left(-\xi^2\right)\left[c_2\left(\exp\left(\xi^2\right)-\exp\left(\eta^2\right)\right)+|c_3|\gamma_k\exp\left(\eta^2\right)\right]\\ &+ (c_1c_2-c_3)\sqrt{\pi}\exp\left(\eta^2\right)[\mathrm{Erf}(-\eta)-\mathrm{Erf}(\xi)]\Big\}, \quad \text{if } c_3>0\\ \gamma(t') = \frac{1}{|c_3|s}\Big\{&s\exp\left(-\eta^2\right)\left[c_2\left(\exp\left(\xi^2\right)-\exp\left(\eta^2\right)\right)+|c_3|\gamma_k\exp\left(\xi^2\right)\right]\\ &+ (c_1c_2-c_3)\sqrt{\pi}\exp\left(-\eta^2\right)[\mathrm{Erfi}(-\eta)-\mathrm{Erfi}(\xi)]\Big\}, \quad \text{if } c_3<0\end{aligned} \tag{A9}$$

where

$$s \equiv \sqrt{2a\sigma_k|c_3|}, \quad \xi \equiv c_1/s, \quad \eta \equiv (c_3t'-c_1)/s, \quad \mathrm{Erfi}(z) \equiv \mathrm{Erf}(iz)/i \tag{A10}$$

i being the imaginary unit ($i^2=-1$). From the definition of the imaginary error function Erfi(.) it emerges that the solution (A9) is a real-valued function also when $c_3<0$. For instance, the case $c_3<0$ is accomplished during inflation time intervals ($V(t)>0$) for the PN configuration, basically due to opposite signs in shear and normal stressing rates (positive and negative, respectively; see Section 3 for details).

Appendix B. Supplementary material

Supplementary material to this article can be found online at doi:10.1016/j.epsl.2010.12.015.

References

Amoruso, A., Crescentini, L., Berrino, G., 2008. Simultaneous inversion of deformation and gravity changes in a horizontally layered half-space: evidence for magma intrusion during the 1982–1984 unrest at Campi Flegrei caldera (Italy). Earth Planet. Sci. Lett. 272, 181–188.

Anderson, E.M., 1905. The dynamics of faulting. Trans. Edinb. Geol. Soc. 8, 387–402.

Aster, R.C., Meyer, R.P., 1988. Three-dimensional velocity structure and hypocenter distribution in the Campi Flegrei caldera, Italy. Tectonophysics 149, 195–218.

Belardinelli, M.E., Bizzarri, A., Cocco, M., 2003. Earthquake triggering by static and dynamic stress changes. J. Geophys. Res. 108 (No. B3), 2135. doi:10.1029/2002JB001779.

Berrino, G., 1998. Detection of vertical ground movements by sea-level changes in the Neapolitan volcanoes. Tectonophysics 294, 323–332.

Berrino, G., Gasparini, P., 1995. Ground deformation and caldera unrest. Cah. Cent. Eur. Geodyn. Séism. 8, 41–55.

Bizzarri, A., Cocco, M., 2006. A thermal pressurization model for the spontaneous dynamic rupture propagation on a three-dimensional fault: 2. Traction evolution and dynamic parameters. J. Geophys. Res. 111, B05304. doi:10.1029/2005JB003864.

Bonafede, M., Trasatti, E., Giunchi, C., Berrino, G., 2010. Geometrical and physical properties of the 1982–1984 deformation source at Campi Flegrei. Geophys. Res. Abstr. 12 EGU2010-5029.

Catalli, F., Cocco, M., Console, R., Chiaraluce, L., 2008. Modeling seismicity rate changes during the 1997 Umbria–Marche sequence (central Italy) through a rate- and state-dependent model. J. Geophys. Res. 113, B11301. doi:10.1029/2007JB005356.

Cocco, M., Hainzl, S., Catalli, F., Enescu, B., Lombardi, A.M., Woessner, J., 2010. Sensitivity study of forcasted seismicity based on Coulomb stress calculation and rate- and state-dependent frictional response. J. Geophys. Res. 115, B05307. doi:10.1029/2009JB006838.

De Natale, G., Zollo, A., Ferraro, A., Virieux, J., 1995. Accurate fault mechanism determinations for a 1984 earthquake swarm at Campi Flegrei caldera (Italy) during an unrest episode: implications for volcanological research. J. Geophys. Res. 100, 24167–24185.

Del Gaudio, C., Aquino, I., Ricciardi, G.P., Ricco, C., Scandone, R., 2010. Unrest episodes at Campi Flegrei: a reconstruction of vertical ground movements during 1905–2009. J. Volcanol. Geotherm. Res. 195, 48–56.

Dieterich, J., 1994. A constitutive law for rate of earthquake production and its application to earthquake clustering. J. Geophys. Res. 99, 2601–2618.

Dieterich, J., Cayol, V., Okubo, P., 2000. The use of earthquake rate changes as a stress meter at Kilauea volcano. Nature 408, 457–460.

Feuillet, N., Nostro, C., Chiarabba, C., Cocco, M., 2004. Coupling between earthquake swarms and volcanic unrest at the Alban Hills Volcano (central Italy) modeled through elastic stress transfer. J. Geophys. Res. 109, B02308. doi:10.1029/2003JB002419.

Gaeta, F.S., Peluso, F., Arienzo, I., Castagnolo, D., De Natale, G., Milano, G., Albanese, C., Mita, D.G., 2003. A physical appraisal of a new aspect of bradyseism: the miniuplifts. J. Geophys. Res. 108 (B8), 2363. doi:10.1029/2002JB001913.

Gomberg, J., Reasenberg, P., Cocco, M., Belardinelli, M.E., 2005. A frictional population model of seismicity rate change. J. Geophys. Res. 110, B05S03. doi:10.1029/2004JB003404.

Gottsmann, J., Berrino, G., Rymer, H., William-Jones, G., 2003. Hazard assessment during caldera unrest at the Campi Flegrei, Italy: a contribution from gravity–height gradients. Earth Planet. Sci. Lett. 211 (3–4), 295–309.

Linker, M.F., Dieterich, J.H., 1992. Effects of variable normal stress on rock friction: observations and constitutive equations. J. Geophys. Res. 97, 4923–4940.

Orsi, G., Civetta, L., Del Gaudio, C., De Vita, S., Di Vito, M.A., Isaia, R., Petrazzuoli, S.M., Ricciardi, G.P., Ricco, C., 1999. Short-term ground deformations and seismicity in the resurgent Campi Flegrei caldera (Italy): an example of active block-resurgence in a densely populated area. J. Volcanol. Geotherm. Res. 91, 415–451.

Rinaldi, A.P., Todesco, M., Bonafede, M., 2009. Hydrothermal instability and ground displacement at the Campi Flegrei caldera. Phys. Earth Planet. Inter. 178, 155–161. doi:10.1016/j.pepi.2009.09.005.

Ruina, A.L., 1983. Slip instability and state variable friction laws. J. Geophys. Res. 88, 10,359–10,370.

Satriano, C., Capuano, P., De Matteis, R., Pasquale, G., Zollo, A., 2009. Earthquakes location and stress field inversion for the 1984 seismic crisis at Campi Flegrei caldera (Southern Italy). Geophys. Res. Abstr. 11 EGU2009-4558-1.

Toda, S., Stein, R.S., Sagiya, T., 2002. Evidence from AD 2000 Izu islands earthquake swarm that stressing rate governs seismicity. Nature 419, 58–61.

Troise, C., Pingue, F., De Natale, G., 2003. Coulomb stress changes at calderas: modeling the seismicity at Campi Flegrei (southern Italy). J. Geophys. Res. 108 (B6), 2292. doi:10.1029/2002JB002006.

Wang, R., Lorenzo-Martín, F., Roth, F., 2006. PSGRN/PSCMP — a new code for calculating co- and post-seismic deformation, geoid and gravity changes based on the viscoelastic-gravitational dislocation theory. Comput. Geosci. 32, 527–541.

Zuppetta, A., Sava, A., 1991. Stress pattern at Campi Flegrei from focal mechanisms of the 1982–1984 earthquakes (Southern Italy). J. Volcanol. Geotherm. Res. 48, 127–137.